JOURNAL OF SPACECRAFT AND ROCKETS
Vol. 31, No. 6, November–December 1994

Computer Experiments on Arcing Processes as Observed in Ground Tests

Heinz Thiemann*
Arbeitsgruppe Weltraumforschung und -Technologie, D-79098 Freiburg, Germany
and
Robert W. Schunk†
Utah State University, Logan, Utah 84322-4405

Experiments with negatively biased solar arrays have shown the edge region to be susceptible to arcing. This suggests the possibility of shorts between the conductive or semiconductive solar-cell edge parts and the conductive carbon fiber substrate through the thin Kapton foil. The interconnect region appears to be less critical. Computer simulations verify that the electrical characteristics of the solar-cell–Kapton–carbon-fiber substrate interface are sensitive to arcing. Strong differential potentials form across the array surface, due to particular charging processes on the different materials. An avalanche of secondary processes near the cell-Kapton edge generates an explosive current flow between these neighboring locations on the array. Strong electric fields also form near the cover-glass–interconnect–cover-glass interface. However, the lack of charged particles in the vicinity of this interface yields rather benign conditions, and hence no energy release.

I. Introduction

VARIOUS laboratory experiments dealing with simulated low-earth-orbit (LEO) plasmas have confirmed the occurrence of arcing near solar-cell edges for negatively biased solar-array test modules.[1] It also has been found that the arcing rate near the interconnectors is negligible at low voltages ($|V| < 500$ V), which are representative of LEO conditions. Moreover, the critical locations has been identified to be the small conductive or semiconductive parts in the cell that are exposed to the space environment.[2] Even if one intends to insulate all parts of the solar array, the insulation will never be perfect, leaving exposed small conductive areas. Breakdowns or discharges will probably occur because of a differential charge buildup. The charge buildup typically produces an electric field that exceeds a breakdown threshold at some point. When a discharge occurs, charge flows from a part of the spacecraft to another part or to space. This charge release will continue until the differential driving force no longer exists. Hence, the amount of charge released will be controlled by the total charge stored in or on the discharge site.[3]

Experimental tests performed in the negative voltage range of several hundred Volts[1] showed the following features:

1) Transient currents flowed between the test sample and the chamber ground through the plasma. Currents of fractions of amperes were anticipated during a brief time period of less than a millisecond; the tests were not designed to resolve the magnitude and duration of the current peaks.

2) The current peaks were correlated with arc discharges near the solar-cell edges and not around the interconnects.

3) The arc discharges lead to carbonization of the Kapton, which loses its insulation property at the arc location.

In this paper, we present numerical results on simulated arcing processes in the solar-cell edge region, using a self-consistent theoretical treatment of the dynamical plasma evolution. The simulation demonstrates that the specific electrical configuration around the solar-cell edge region, in association with the plasma environment and secondary electron emission processes, is adverse to solar-array operation in the negative voltage range.

Received Oct 30, 1992; revision received Dec. 18, 1993; accepted for publication May 16, 1994.

*Senior Research Scientist.

†Director, Center for Atmospheric and Space Sciences.

A. Description of Critical Locations

Figure 1 is a schematic diagram of a typical solar-array test module used for laboratory interaction experiments in a simulated LEO-plasma environment. The dominant location for arc discharges, labeled 1 in Fig. 1, is the edge region, where no interconnects are present. The interconnect region, on the other hand, is labeled 2. This region describes a noncritical location for arcing, according to ground tests[4] and computer experiments.[5]

A cross section of each region is shown in Fig. 2. Conductors are marked by black areas, semiconductors by hatched areas, and dielectric parts by grey areas. We do not consider the complete details of combined dielectric structures of a realistic array (e.g., cover glass glued with dielectric adhesives to the cell or substrate dielectrically glued to the honeycomb, etc.), but for simplicity treat only the bulk dielectric behavior.

A relevant edge region is encircled in Fig. 2 (upper diagram). The actual surfaces exposed to the plasma are (from left to right) dielectric cover glass, semiconductive cell, and Kapton surface. The cover slides are attached to the metallic grid fingers that lead to the interconnects. Hence, they become polarized and reach surface potentials of the order of the applied interconnect voltage. Consequently, the internal electric fields are initially small. The semiconductive cell is also connected to the interconnects. This part is composed of a biased conductor, the semiconductive cell, and another conductor that leads to the next interconnect. We call this the cell for convenience, and we treat it as a biased conductor with corresponding emission properties. At basically the same potential, it will behave like a conductor. Finally, the Kapton is on top of the metallic honeycomb or carbon fiber structure. Connected to the main spacecraft, the potential of this conductor will reflect the charging in the presence of the thermal plasma, and it will be slightly negative (typically -0.5 to -1 V). The Kapton surface far from the cell will reach comparable potentials. Only close to the cell will the high potential of the cell influence the Kapton surface to some extent. In the initial stage, the cover glass and semiconductor are therefore at high negative potentials, and the Kapton is at a reduced negative or zero potential. Hence, initially, there is a significant voltage drop between the cell and the Kapton.

The interconnect region in Fig. 2 (lower diagram) has different electrical characteristics than the edge region. Here, the exposed surfaces are symmetric around the central interconnect with one cover slide on each side. The influence of the substrate is of minor importance. Initially, the whole boundary is almost an equipotential surface, with similar potential values over the different electrical

materials. In the edge region, new features are introduced by the Kapton insulation foil material, which is directly exposed to the plasma environment. The fundamentally different electric field conditions in the edge and interconnect regions will significantly control the charged-particle flow to the surfaces, and therefore also the charging and discharging processes on the surfaces as well as the secondary-emission effects.

B. Simulation System

The dynamic evolution of the interactions is controlled by electrical boundary conditions, the plasma parameters, and the secondary electron emission properties. Background gas ionization is not considered at present.

1. *Boundary Conditions*

The actual electrical boundary conditions at the interconnect and edge regions, as shown in Fig. 2, have to be simplified for a numerical model.[6] Since the interconnect boundary is similar to the edge boundary, we only discuss the basic ingredients of the boundary condition at the edge. The idealized surfaces used for our simulations are shown at the bottom of Figs. 3 and 4. The edge region is characterized by three electrically different parts: the dielectric cover slide, the conductive or semiconductive cell, and the dielectric Kapton. The model in Fig. 4 simplifies the real situation (Fig. 2) in defining a planar geometry. For that purpose, we rotate the cell side into the coverslide-Kapton plane.

Coverslide. The boundary condition at the surface of the coverslide is given by the electric field discontinuity at the corresponding grid points:

$$E_{cs}^{+} - \varepsilon_{cs} E_{cs}^{-} = \sigma_{cs}^{ext} \tag{1}$$

The electric field in the cover slide, $E_{cs}^{-} = (\Phi_c - \Phi_{cs})/d_{cs}$, is initially close to 0, with the surface potential Φ_{cs} slightly smaller than the interconnect potential $\Phi_c = -250$ V. The potential Φ_c represents the applied fixed potential of the metallic grid fingers beneath the cover glass, and Φ_{cs} is the surface potential of the cover-slide, which evolves according to the surface charges. We select a cover-slide thickness of $d_{cs} = 100\ \mu$m and a permittivity of $\varepsilon = 4$. The external charges σ_{cs}^{ext} result from the plasma particle flow and the secondary particle emission. The outer electric field is defined by $E^{+} = (\Phi_{cs} - \Phi_1)/\Delta y_1$, where Δy_1 and Φ_1 correspond to the width of the first grid cell in front of the surface and the related potential at this point, respectively.

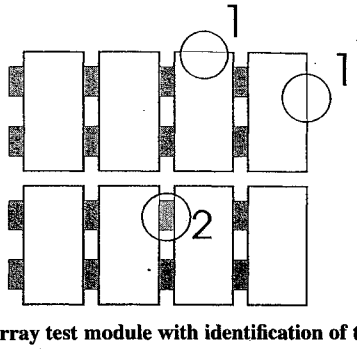

Fig. 1 Solar-array test module with identification of the edge (1) and interconnect (2) regions.

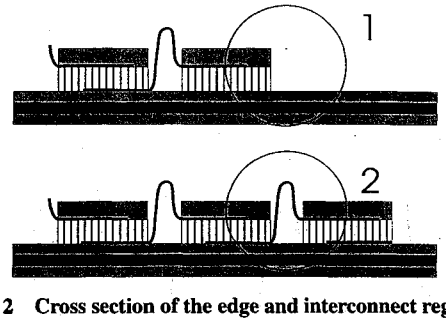

Fig. 2 Cross section of the edge and interconnect regions.

Semiconductive cell. As mentioned before, the cell is treated electrically as a conductor with a fixed voltage of typically $\Phi_c = -250$ V, which is equal to the interconnect value.

Kapton insulation layer. The potential of a conductive structure in the LEO-plasma environment is ≤ 0 V. The Kapton insulation layer is then described by a boundary condition that is similar to that of the cover glasses,

$$E_{Kapton}^{+} - \varepsilon_{Kapton} E_{Kapton}^{-} = \sigma_{Kapton}^{ext} \tag{2}$$

The electric field in a Kapton sheet of thickness d_{Kapton}, given by $E_{Kapton}^{-} = (\Phi_{structure} - \Phi_{Kapton})/d_{Kapton}$, initially has a significant magnitude close to the cell, where the fixed potential bias of the cell is dominant. The field decreases in the Kapton layer as one moves away from the cell. The potential $\Phi_{structure}$ represents the structure potential of ~ 0 V, and Φ_{Kapton} is the surface potential of the Kapton. The external charges, σ_{Kapton}^{ext}, again result from the plasma particle flow and the secondary-particle emission from the Kapton surface.

2. *Secondary Emission*

Impacting electrons and ions with appropriate energies cause secondary-electron emission from the material surfaces at a prescribed, material-specific rate. The material emission properties have been widely investigated. The emission properties of the cover slides are determined by the antireflection coating material MgF_2. Laboratory experiments have provided the yield versus particle energy.[7] The experimental results are well approximated by the expression (with E in electron volts)

$$Y_{MgF_2} = \sqrt{0.036E} \tag{3}$$

for $E < 400$ eV. Conductive materials generally have a lower emission yield than dielectrics. A typical emission yield is given by experiments studying aluminum emission properties,[8]

$$Y_{Al} = 1.1(e^{-0.1E} - e^{-10E}) \tag{4}$$

The emission yield of Kapton is well known[8] and is given by the analytical formula

$$Y_{Kapton} = 3.5(e^{-2E} - e^{-15E}) \tag{5}$$

The additional possibility of secondary electron emission from the Kapton surface has not previously been suggested with respect to the interconnect region.

Secondary electron emission caused by ion impact is not as well understood as electron-induced secondary emission. However, it is known that even very slow ions generate secondary electrons.[9] For our purpose, we assume that the secondary electron generation is dependent on the energy of the incident ion. We use typical electron yield relations given in the literature.

The dependence of the emission yield on the angle of incidence of the charged particles is not included in our simulations. It is known that oblique impact on surfaces causes enhanced emission. Our calculations, therefore, will give a lower limit for emission. The velocity of the emitted particles parallel to the surface is derived from a Maxwellian plasma distribution, and the velocity perpendicular to the surface from a half-Maxwellian distribution.

3. *Simulation System*

Typical parameters of the LEO environment are given in Table 1. The plasma density, plasma frequency, electron thermal energy, and the Debye shielding length are used as normalization values in our numerical scheme. We determine the relevant values of the simulation with reference to the density, potential, frequency, length, velocity and electric field given in Table 1. For the ions, we use a realistic mass ratio of $m_i = 29{,}400 m_e$. To simulate a moving spacecraft, the electrons and ions are assumed to be drifting towards the solar array surface with a velocity of 8 km/s.

The simulation system is two-dimensional, with x and y coordinates. The system also has a multigrid configuration.[5] The first-order

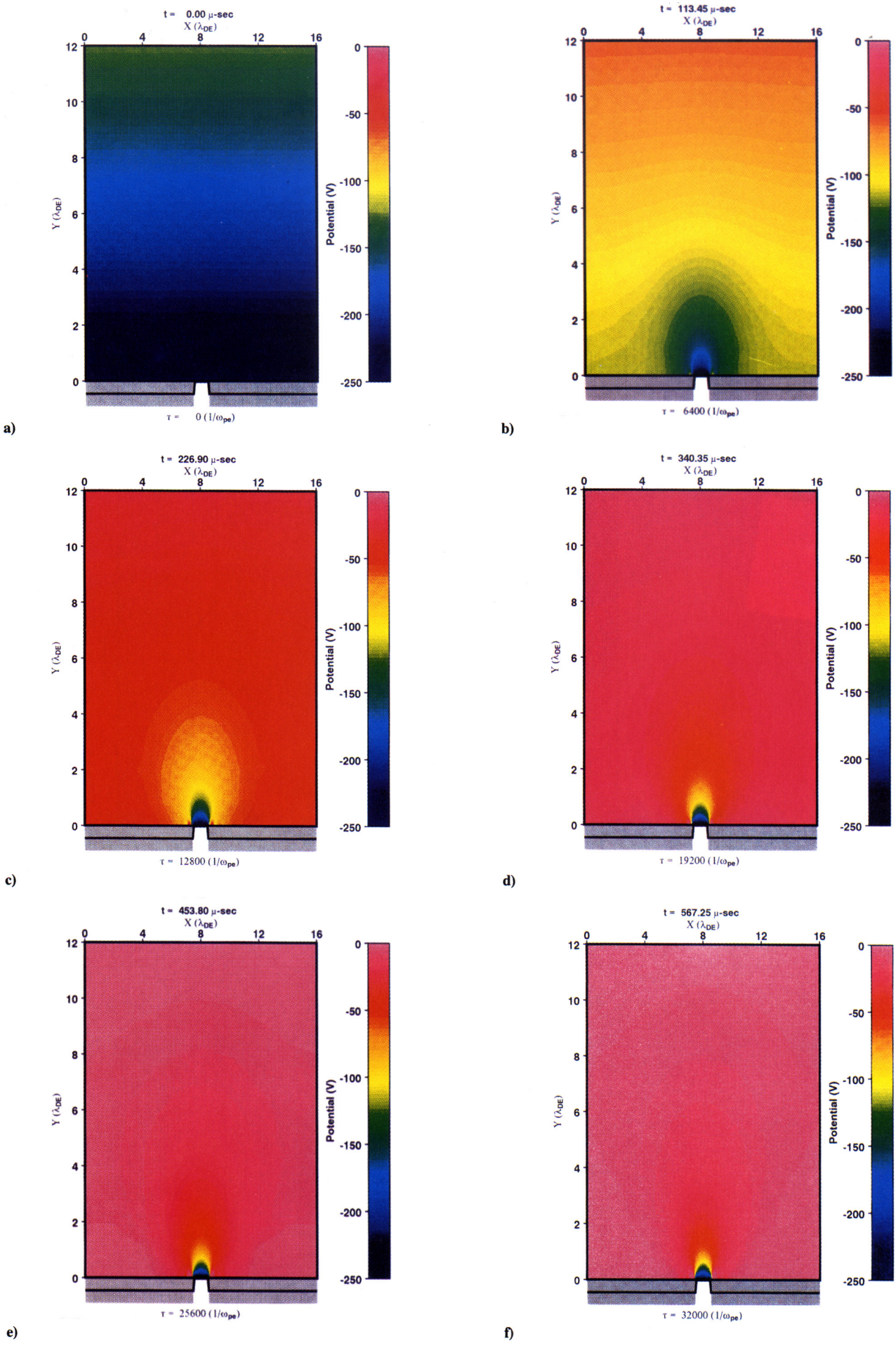

Fig. 3 Snapshots of the potential distribution for the interconnect region at selected times.

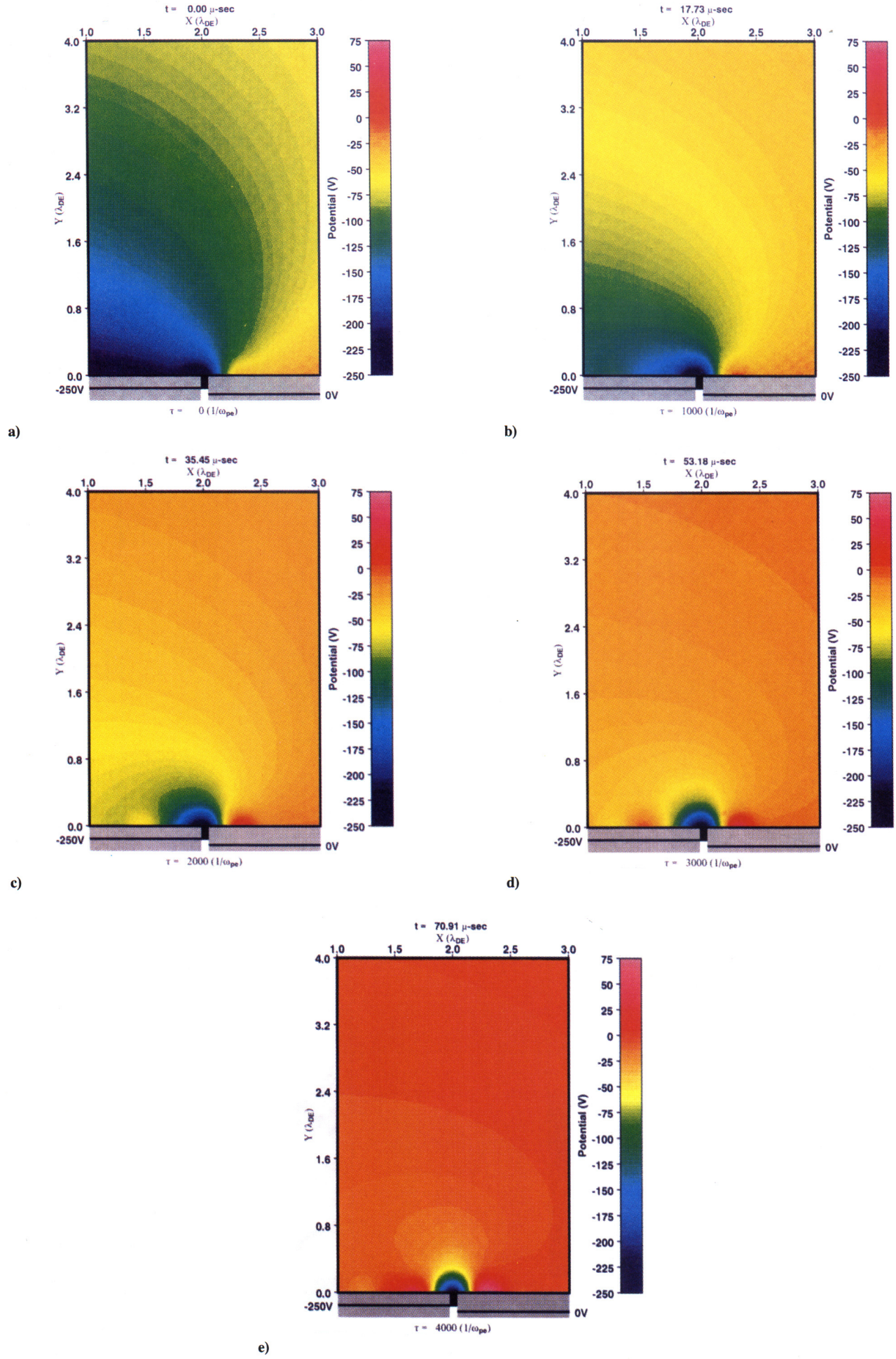

Fig. 4 Snapshots of the potential distribution for the solar–cell–Kapton interface region at selected times.

Table 1 Characteristic parameters of the LEO ionosphere

n_0	10^6 cm^{-3}
$\Phi_0 = kT_e/e$	0.05
ω_{pe}	56.5 MHz
λ_{de}	0.166 cm
v_{te}	9.4×10^4 m/s
$E_0 = \Phi_0/\lambda_{de}$	0.3 V/m

grid has a cell size of λ_{de} in both directions, with $x_{max} = 16\lambda_{de}$ along the model array surface and $y_{max} = 96\,\lambda_{de}$ extending into the plasma environment. The two cells above the numerical-array boundary are overlaid with a fine grid that has a mesh size of $\lambda_{de}/4$. The interesting transition region between the cover slide, cell, and Kapton has a similar mesh refinement in the vertical direction. For the edge region, we apply an overall mesh refinement, while the system lengths remain the same in the x and y directions. The width of the biased cell corresponds to the width of one numerical grid cell of the fine grid, $\Delta_x = 0.25\lambda_{de}$. This corresponds to a width of 420 μm, which is close to realistic values of 200–300 μm.

The potentials at the lower boundary are determined according to the discussion in Sec. II.B.1, and the upper boundary is fixed at a potential of 0 V, which describes the undisturbed plasma environment. The lateral boundary conditions are periodic.

Initially, at $t = 0$, the system is uniformly filled with 16 thermal electrons and ions per Debye cell, which defines quasineutrality at the beginning. The electric fields are then determined only by the chosen boundary conditions. The charged particles are advanced by the particle-in-cell technique[5] according to their interaction with the fields. The time increment of our simulation is $\Delta t = 0.0125\omega_{pe}^{-1} = 0.2$ μs, which is chosen in order to guarantee that particles do not move more than one cell during one pushing process in the large-electric-field region near the array cell. Particles that hit the lower boundary contribute to the surface charge at the corresponding location. New particles are supplied from the top according to the following scheme. The number of thermal electrons and ions is adjusted in the first four upper cells in order to maintain quasineutrality with field-free conditions at the top of the system. After particle pushing, space charges accumulate at various locations in the system and surface charges accumulate on the array surface, which in turn results in a general modification of the overall electric field distribution. With the new fields, the particle pushing mechanism is repeated, etc.

II. Results

In the following, we compare the temporal evolution of the potential distribution around the interconnect and edge regions. For the interconnect region, we present results in more detail than have been already presented.[10]

A. Interconnect Region

Figure 3a shows the potential distribution at $t = 0$ s, for the case where a voltage $\Phi_0 = -250$ V is suddenly applied to the interconnect, which is at the center. At this instant, the surrounding plasma is still quasineutral and has no effect on the potential distribution, which is completely determined by the boundary conditions. A schematic sketch of our boundary model of this part of the array surface is provided at the bottom of the figure. We only show the interesting part of the simulation system where pronounced potential structures occur. Note that the polarization of the cover slides results in only slightly reduced surface potentials. This leads to an almost planar potential distribution everywhere in the system. As time elapses (Figs. 3b to 3f), contracting potential lenses form around the interconnect region. In the quasistationary state around $t = 400$–480 ms (Fig. 3f), very confined and nearly symmetric structures extend about $3\lambda_{de}$ (= 5 mm) along the surface and $6\lambda_{de}$ (= 10 mm) into the plasma. The cover-slide potential basically settles at 0 V. Outside the pronounced potential lens, almost field-free conditions are obtained.

The temporal evolution of the potential distribution suggests the following scenario. Initially, only ions flow to the target surface, while electrons move in the opposite direction. The ions contribute to the current collected by the interconnect and to the discharging of the negative polarization charges on the cover glass. This leads to a decrease in the magnitude of the negative surface potential and a final adjustment to a value of 0 V. As the potential lenses gradually form, they focus the bulk of the inflowing plasma ions to the interconnect and prevent further charging of the dielectric surfaces. The field-free outer space allows refilling with thermal plasma electrons. Because of their small thermal energy (0.05 eV), the charging of the dielectric surfaces by these electrons is negligible. The thermal electron dynamics is therefore of minor importance for interactions in the interconnect region.

The secondary electron emission associated with energized ions impacting on the dielectric surfaces is only operative in the beginning, when large negative potentials exist. On most of the cover glass, the electric fields are almost vertical, which acts to accelerate secondary electrons away from the array. Near the interconnect, the fields also repel the electrons, which finally are diverted to the undisturbed environment. The emission of negative charges, on the other hand, leaves positive surface charges, which further speeds up the discharging of the cover slides. With the reduction of the surface potential, the emission from the cover slides subsides as time proceeds. Finally, this process is completely stopped. Electron emission from the interconnect, however, continues during the whole simulation. These electrons, which are emitted from the conductor at a relatively low rate, flow into the ambient plasma because of the strong perpendicular electric fields near the interconnect.

Although strong electric fields form in the interconnect–cover-glass environment, the secondary electrons are not able to interact with adjacent parts of the array surface. With no particle flow from the interconnect to the cover glass, this interaction is rather benign and not harmful to the operation of the array.

B. Edge Region

Snapshots of the potential structures for the edge region are shown in Fig. 4. Since the potential structures evolve on very small scale lengths, we further zoom in on the interesting part of the simulation system. In this figure, we only show the region close to the cell. The model of the target boundary, which idealizes the cross section of Fig. 2 (upper diagram), is shown at the bottom of this figure. The reference potentials for the cover slide (−250 V) and the Kapton foil (0 V) are indicated. With the lateral and top boundary conditions maintained, the new bottom boundary (cover-glass–cell–Kapton) introduces significantly different interaction processes.

Figure 4a shows the vacuum conditions with the quasineutral plasma environment. In the initial state, the potential structures differ completely from the planar structures of the interconnect environment. Here, the equipotential contours extend in an almost vertical direction from the cell into the plasma. Only far from the target surface do the potential contours become horizontally inclined. Although the cover-slide surface is again almost an equipotential at the cell potential, the Kapton is influenced by the nearby cell. This acts to counteract the effect of the carbon-fiber reference potential and generates a negative surface potential on the Kapton edge, which decreases from the cell outwards. During the temporal evolution of the interaction (Figs. 4b–4e), distinct small-scale potential structures form in the vicinity of the cell. At $t = 70.9$ μs, the surface shows a very efficient shielding within $2\lambda_{de} = 3.3$ mm. On the Kapton side, positive-potential cusps form for $t > 35.45$ μs. Similar structures are also seen on the cover glass for $t > 64$ μs, although with smaller values. Outside the pronounced potential structures, almost electric-field-free conditions are established, which allows an inflow of plasma particles from the undisturbed environment.

The initial electric fields, related to the potentials of Fig. 4a, produce a downward acceleration of ions near the cover glass. Polarization of the cover glass initially generates negative surface charges, which are subsequently discharged by inflowing ions and secondary electron emission. This process is comparable to the situation in the vicinity of the interconnect.

Near the Kapton, an initial transient effect occurs. Ions are not able to reach the Kapton surface on account of the initial oppositely

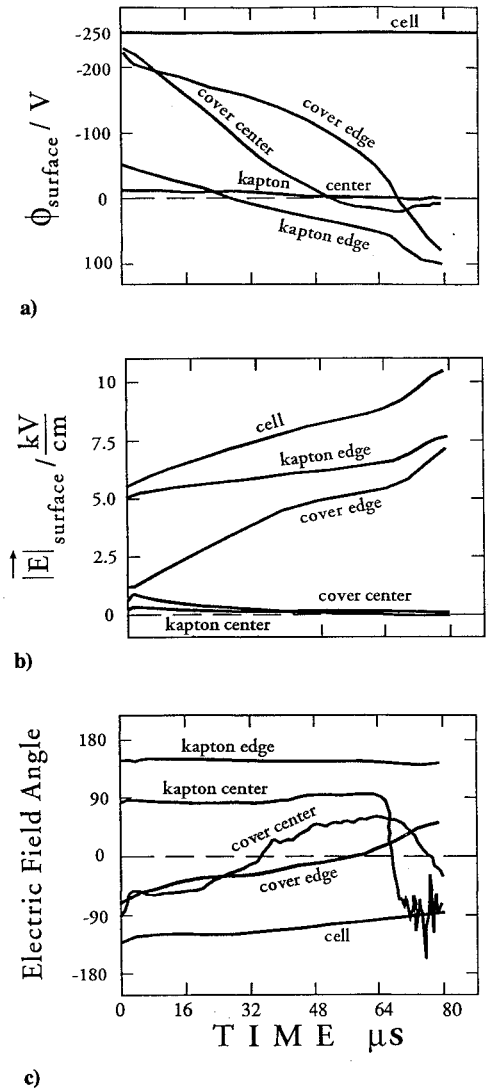

Fig. 5 a) Temporal evolution of the surface potential, b) the magnitude of the electric field, and c) the direction of the electric field at different locations on the target.

directed electric fields (Fig. 4a). Only electrons moving in these electric fields can reach the surface. During the interaction, this condition is modified. The asymmetric behavior of the potential contours is maintained during the whole simulation. Consequently, ions are able to reach different parts of the target surface at later times (e.g., Fig. 4e). This is a basic difference from the potential distribution in Fig. 3 for the interconnect region, where ions are only attracted by the interconnect.

Figure 5a shows the temporal evolution of the potentials at different locations on the target surface. There are three different groups of curves, which refer to the cell, the cover glass, and the Kapton. Two locations are selected on the cover slide and Kapton, respectively, to show the potential behavior close to and far from the cell. Initially, all potentials are negative. The cell is biased at the fixed voltage of −250 V during the whole interaction. The cover glass shows, initially, similar values of around −220 to −230 V over the entire surface, while the Kapton potential is lower, at about −40 V. We note that the discharging is most pronounced in the vicinity of the cell, with positive potentials after $t > 64$ μs. The small surface potentials beyond this region depict the efficient shielding of the cell environment.

The magnitudes of the related electric fields vs time are shown in Fig. 5b. The largest fields are observed on the cell. Outside, the most dominant fields develop at the cell-Kapton interface. The fields near the cover-slide–cell interface are initially small, but increase to values comparable to those at the edge during the interaction. Far from the cell, the fields on both dielectric surfaces are insignificant. For the particle dynamics, we also have to consider the field direction. In Fig. 5c, we show the angle of the electric field vector. Here, −90 and +90 deg refer to vertical directions, pointing downward and upward, respectively. The field on the cell always points downward. Initially, it is inclined at an angle of about −130 deg and finally approaches −90 deg, i.e., a orientation. The field adjacent to the cover glass also points downward initially. After $t \geq 55$ μs, it reverses its direction. At this time, we also observe a more intense charging in the surface potential (Fig. 5a).

The electric field at the part of the Kapton near the cell always points upward, with an almost constant inclination of +140 deg. Further from the cell, the field direction changes significantly. However, because of the small magnitude of the electric field at these locations (Fig. 5b), this does not have a major effect on the operation of the array.

The main feature seen in Fig. 5c is the very pronounced field reversal within a short distance in the cell-Kapton transition region. A similar field reversal also develops between the cover glass and cell at the end of the run, after the polarization charges are neutralized by the inflowing ions and associated emitted secondary electrons.

The simulations show the existence of electrons that participate in the interaction with the boundary. Such electrons, however, cannot originate in the plasma. Because of their low thermal velocities, plasma electrons are not able to overcome the potential barrier of ~ −10 V (Fig. 4e). These electrons are generated by internal secondary emission effects caused by impacting charged particles of sufficient energy. Therefore, in Fig. 6a, we show the difference of impacting ions and associated secondary electrons at various locations on the target surface. The curves represent the flux accumulated during the temporal evolution. A negative slope in Fig. 6a refers to more emitted electrons than impacting ions. A strong decrease implies rather energetic ions with a very intense emission. A positive slope describes missing or reduced electron emission from ion impact. The horizontal part means essentially no ion deposition.

Figure 6a demonstrates the discharging process on the cover glass. This process starts far from the cell on the cover glass. Inflowing ions, impacting on the surface, create secondary electrons with a large yield up to $t = 56$ μs. With an efficient supply of positive surface charges via ion deposition and electron emission, the surface potential at this location (Fig. 5a) is in agreement with this observation. For $t > 56$ μs there is no significant flow of ions to this location. At locations close to the cell, the discharge proceeds at a slower rate. Only after the discharging of the neighboring locations stops do we observe (at $t > 64$ μs) a strong decrease of the curve, characterizing the cover-slide location close to the cell. This is again in agreement with the related surface potential in Fig. 5a. With regard to the cell, it displays similar features, with enhanced secondary electron emission after $t > 64$ μs. This, of course, has no effect the potential.

The ion flow to the Kapton surface appears to be not very prominent. Indeed, this is true for the bulk of the Kapton surface. Therefore, we only show the location close to the cell in Fig. 6a. The corresponding curve decreases only slightly, which means the impacting plasma ions have an electron yield $Y > 1$. Towards the end of the run, the curves approach a horizontal line; therefore ions can no longer reach this location. During the continuous charging process, which turns out to be quite substantial, polarization charges do not have to be neutralized at this location. The effect is seen in Fig. 5a in the behavior of the associated surface potential curve. The electric field directions near the cell-Kapton interface in Fig. 5c confirm that ions are attracted under oblique incidence. With the ongoing charging of this location, the potential increases and the potential step between the cell and Kapton becomes successively steeper and more pronounced. Finally, the electric field direction in front of the cell becomes vertical (Fig. 5c) and acts to attract all inflowing ions. The ion flow to the Kapton is then interrupted. Consequently, the surface potential becomes constant (Fig. 5a).

We should emphasize here that the granularity of our grid introduces some numerical errors near the cell-Kapton interface. As long as ions hit the dielectric Kapton near the cell, they contribute to the surface charge of the first grid point on the Kapton, even if

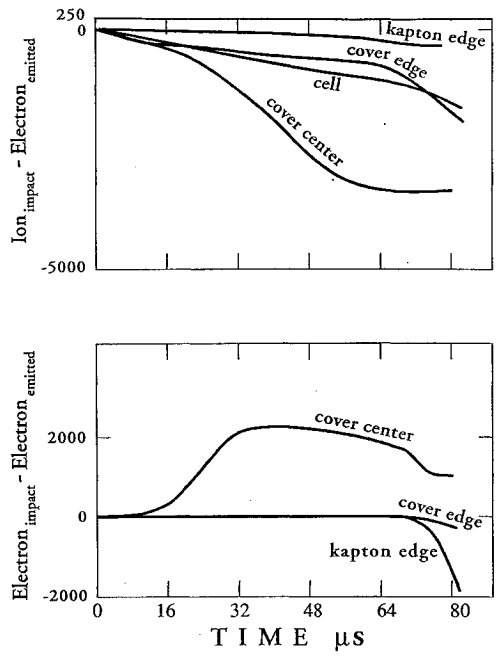

Fig. 6 a) Difference of impacting ions and associated secondary electrons and b) of impacting electrons and associated secondary electrons.

the point of impact is very close to the cell. This numerical effect is also present in calculations involving a higher grid resolution and cannot be eliminated. Therefore, we get slightly higher charging at this point than in reality, where the potential step will be still steeper. With a steeper potential step, the flow of ions to adjacent Kapton surfaces will stop earlier than we predict. In our calculations, the ion flow to this location is also eventually terminated by the perpendicular electric field in front of the cell. The qualitative results of our simulation are therefore still valid. A similar consideration applies for the first grid point on the cover slide (left side of the cell).

An interpretation similar to that for Fig. 6a applies for the difference of impacting electrons and associated secondary electrons, shown in Fig. 6b. A positive slope describes electron deposition without secondary emission. Negative slopes characterize the dominance of emitted electrons. A horizontal line again means no electron inflow at the corresponding location. In the center of the coverglass, we observe the onset of electron deposition for 16 μs $< t <$ 24 μs. Here, we deal with low-energy electrons. The gradual discharging of the surface towards the cell generates a potential gradient across the surface (e.g., Fig. 4b). All ions impacting near the cell at this time produce secondary electrons. According to the potential structures shown in Fig. 4b, these secondaries are reflected back to the cover-slide surface at a more distant location. Since the potential difference is only a few tens of volts, their energy is not sufficient to cause additional secondaries. Thus, the effect of a net negative surface charge is achieved. At $t >$ 72 μs, a brief time interval of increased emission due to impacting electrons is observed, which results from electron emission from the cell. The electric fields corresponding to Fig. 4f show the effect of these electrons by creating a larger potential difference.

Finally, however, the emission is most concentrated in the immediate environment of the cell. Near the cell on the cover-glass side, the emission process is only significant for $t >$ 76 μs, when secondary electrons generated at the cell are able to generate secondaries themselves on the cover slide by passing through the large potential drop that exists between these locations. However, it is evident from the strong electric fields seen in Fig. 5b that most of the secondaries generated at that time on the cell are diverted to the adjacent Kapton surface, as can be seen from Fig. 6b.

III. Conclusions

Our computer experiments demonstrate the formation of a differential charge buildup and associated differential potentials on solar arrays. The different materials on the solar-array surface are characterized by different electrical potential conditions both initially and during the temporal evolution of the plasma-array interaction. The interaction also dynamically modifies the potential distribution in the vicinity of the array, which in turn modifies the particle flow to the array and the associated secondary electron emission. Our simulations indicate that the plasma flow and emission processes are distinctly different in the interconnector and edge regions, with the edge being more susceptible to arcing.

Initially, the solar array is subjected to an almost constant ion flow over the different materials of the surface. The dielectric cover glasses, with negative reference potentials of −250 V, are polarized to generate negative surface potentials. On the cover slides, attracted ions cause a gradual discharging of the cover-glass surface, by counteracting the negative polarization charges. Secondary electrons emitted from this location are accelerated away from the surface due to the almost perpendicular electric fields. The electron emission leaves positive surface charges and leads to an even more efficient discharging of the dielectric surfaces. This process reduces the magnitude of the surface potential and hence the number of emitted electrons. Eventually, focusing potential lenses form around the interconnect. With the termination of the discharging process, pure ion collection by the interconnect sets in. Subsequently, the secondary electrons emitted from the interconnect are returned to it and are not reflected to a different location on the surface. In the interconnector–cover-glass region, where the secondary emission process stops on the cover slides according to the efficient discharging effect, the source of charged particles is finally eliminated. This region, which is characterized by large electric fields but no particles to initiate a current flow between the critical parts of the interconnector region, is rather benign. This simulation result is in agreement with the experimental results, where no arc discharges are observed[1] near the interconnectors even at voltages as high as −500 V.

For the edge region, a distinctly different potential structure exists near the Kapton-cell interface at the very beginning when the voltage is applied to the interconnect. In response to the complicated potential structures that are associated with this boundary condition, ions flow at different rates to the various locations on the surface. Initially, the ions are predominantly attracted to the cover slides to neutralize the negative surface charges. When the impacting ions generate secondary electrons, the discharging process is accelerated, and eventually the reduction of the surface potential acts to decrease this ion-induced emission.

In the Kapton insulation foil, substantial polarization is initially prevented by the carbon-fiber potential of about 0 V. However, negative surface potentials result from the influence of the negatively biased cell. Ambient ions are able to flow to the Kapton surface close to the cell, with possible secondary electron emission. Charged particles hitting this surface contribute directly to the Kapton surface charge. The resulting differential potentials become more pronounced during the interaction. Due to the initial boundary conditions, a steep potential step first evolves on the Kapton side. The asymmetry of the outer potential contours allows for a further discharging of the cover slides, which finally also results in a potential step. The potential structures also influence the current-collection characteristics of the cell. Only towards the end of the interaction, when the electric field becomes perpendicular to the cell, are most of the ions attracted to the cell. With an increasing ion collection, secondary emission from this location is also enhanced. The magnitude of the oppositely directed electric fields near the Kapton and its proximity to the biased conductor provide for a more susceptible situation for arcing than on the cover-glass side. This simulation result is in agreement with the experimental results. The secondary electrons are energized by the large electric fields as they flow towards the dielectric Kapton surface. Upon impact, these secondary electrons are also able to generate additional secondary electrons on the Kapton, which substantially increases the current flow to the Kapton surface. With this avalanche type of electron generation, the number of electrons increases dramatically. In our simulation this becomes evident when the number of electrons increases so fast as to cause a blowup of the calculations. Because of the presence of a

large number of electrons in the strong electric fields, a dangerous situation is created at the cell-Kapton interface.

Transient effects are identified by explosive electron emission. The associated currents between the cell edge and the Kapton then temporarily increase to such an extent as to trigger discharges. After such events, the electric properties of these spots on the target are modified and the spots become carbonized Kapton material. The initial target properties are then modified to such an extent that a continuation of the computer simulation for this problem is not meaningful.

Breakdowns or discharges are therefore correlated with differential charges and potential buildups in association with energetic charge carriers flowing between different locations on the solar array surface, especially near the cell-Kapton interface. Ion impact also causes sputtering of slow neutral or ionized particles. With this increase in the neutral- and charged-particle budget in the interaction region, additional processes, such as gas ionization and increased discharge currents, are possible. This latter effect has not been treated in the present study, but is of great interest for new investigations.

References

[1]Thiemann, H., Schunk, R. W., and Bogus, K., "Where Do Negatively Biased Solar Arrays Arc?," *Journal of Spacecraft and Rockets*, Vol. 27, 1990, pp. 563–565.

[2]Hastings, D. E., Cho, M., and Kuninaka, H.,"The Arcing Rate for a High Voltage Solar Array: Theory, Experiment and Predictions," AIAA Paper 92-0576, 1992, pp. 1–27.

[3]Robinson, P. A.,"Spacecraft Environmental Anomalies Handbook," Geophysics Lab., Final Rept. GL-TR-89-0222, Hanscom Air Force Base, MA 01731-5000.

[4]Thiemann, H., and Bogus, K.,"Anomalous Current Collection and Arcing of Solar-Cell Modules in a Simulated High-Density Low-Earth-Orbit Plasma," *ESA Journal,* Vol. 10, 1986, pp. 43–57.

[5]Thiemann, H., and Schunk, R. W., "Particle-in-cell Simulations of Sheath Formation around Biased Interconnectors in a Low-Earth-Orbit Plasma, *Journal of Spacecraft and Rockets,* Vol. 27, 1990, pp. 554–562.

[6]Thiemann, H., and Schunk, R. W.,"Arc Discharges at Negatively Biased Solar Arrays," *Proceedings of the European Space Power Conference,* ESA SP-320, 1991, pp. 589–595.

[7]Levy, L., Sarrail, D., and Signeir, J. M., "Conductivity and Secondary Emission Properties of Dielectrics Required by NASCAP," ESA SP-232, 1985.

[8]Haffner, J. W., "Secondary Electron Effects on Spacecraft Charging," NASA CP-2071, 1978, pp. 756–768.

[9]Massey, and Burhop, *Electronic and Ionic Impact Phenomena,* Oxford Univ. Press, Oxford, England, UK, 1952.

[10]Thiemann, H., and Schunk, R. W.,"Field Formation around Negatively Biased Solar Arrays in the LEO-Plasma," *Advances in Space Research,* Vol. 12, 1992, pp. 143–146.